Borehole-based characterization of deep crevasses at a Greenlandic outlet glacier

Bryn Hubbard[1], Poul Christoffersen[2], Samuel H. Doyle[1], Thomas R. Chudley[2], Charlotte M. Schoonman[2], Robert Law[2], Marion Bougamont[2]

[1]Centre for Glaciology, Department of Geography and Earth Sciences, Aberystwyth University, Aberystwyth, UK. [2]Scott Polar Research Institute, University of Cambridge, Cambridge, UK.

Correspondence to: Bryn Hubbard (byh@aber.ac.uk)

Key Points:

- Borehole logging by optical televiewer reveals the presence of planes, interpreted to be crevasse traces, to a depth of 265 m at Store Glacier, Greenland.
- Crevasses are inferred, from excess ice temperature, to penetrate to a depth of ~400 m.
- Crevasse traces are non-vertical and offset in azimuth from orthogonal to the local direction of principal extending strain, indicating formation by mixed-mode fracturing, probably ~8 km upglacier.
- Crevasse traces show evidence of multiple reactivation phases, indicating that they represent planes of fracture weakness.

Abstract Optical televiewer borehole logging within a crevassed region of fast-moving Store Glacier, Greenland, revealed the presence of 35 high-angle planes that cut across the background primary stratification. These planes were composed of a bubble-free layer of refrozen ice, most of which hosted thin laminae of bubble-rich 'last frozen' ice, consistent with the planes being the traces of former open crevasses. Several such last-frozen laminae were observed in four traces, suggesting multiple episodes of crevasse reactivation. The frequency of crevasse traces generally decreased with depth, with the deepest detectable trace being 265 m below the surface. This is consistent with the extent of the warmer-than-modelled englacial ice layer in the area, which extends from the surface to a depth of ~400 m. Crevasse trace orientation was strongly clustered around a dip of 63° and a strike that was offset by 71° from orthogonal to the local direction of principal extending strain. The traces' antecedent crevasses were therefore interpreted to have originated upglacier, probably ~8 km distant involving mixed-mode (I and III) formation. We conclude that deep crevassing is pervasive across Store Glacier, and therefore also at all dynamically similar outlet glaciers. Once healed, their traces represent planes of weakness subject to reactivation during their subsequent advection through the glacier. Given their depth, it is highly likely that such traces - particularly those formed downglacier - survive surface ablation to reach the glacier terminus, where they may represent foci for fracture and iceberg calving.

Plain language summary Crevasses allow ice-mass motion and the transfer of water and the heat it holds into the ice mass' interior. Crevasses extending deeper than some tens of metres have been inferred from indirect evidence such as radar scattering but have not been observed directly. Here, we evaluate the presence and properties of such deep crevasses by using an optical televiewer (OPTV) to record a continuous high-resolution image of the complete wall of a borehole drilled to a depth of 325 m in Store Glacier, a heavily-crevassed fast-moving outlet glacier of the Greenland Ice Sheet. The OPTV image intersects several now-closed crevasses to a depth of 265 m, many of which show evidence of multiple phases of opening and closing as they have been carried through the glacier to the borehole location. We infer that, at least in fast-moving glaciers such as Store, deep crevasses are pervasive, may be regenerated several times, and are able to transfer water and heat from the surface to depths of at least 400 m. The crevasse traces we image are

sufficiently deep to survive surface melting and reach the glacier terminus. Here, inherited traces could act as planes of weakness, enabling ice fracture and iceberg calving.

1 Introduction

Surface crevassing contributes to bulk ice motion and enables the transfer of water and its thermal energy from the surface of an ice mass to its subsurface. Theoretically, creep closure limits the depth of dry crevasses to some tens of metres (see Mottram & Benn, 2009; Nye, 1955), but this can be increased substantially by hydrofracturing of water-filled crevasses (van der Veen, 1998; Weertman, 1973). Once initiated, hydrofracture extends the tip and, if enough water is available to increase its depth accordingly, propagation can continue to the glacier bed. This mechanism has been used to explain the rapid transfer of meltwater to the glacier bed during discrete surface lake drainage events (e.g., Chudley et al., 2019; Das et al., 2008; Doyle et al., 2013), common through ice up to ~1 km thick around the margins of the Greenland Ice Sheet (GrIS) and at a smaller scale on, for example, Ellesmere Island, Canada (Boon & Sharp, 2003).

In the absence of lake-drainage driving hydraulic fracture, at least four general lines of evidence suggest the presence of deep, englacially-terminating crevasses. First, such crevasses have been considered responsible for englacial warming as a result of energy released by meltwater refreezing within them (e.g., Colgan et al., 2011; Phillips, Rajaram, & Steffen, 2010; Poinar et al., 2017). For example, Lűthi et al. (2015) favoured refreezing of meltwater in 300 – 400 m deep crevasses to explain englacial ice temperatures measured in boreholes near the western margin of the Greenland Ice Sheet. These ice temperatures were recorded to be 10 – 15 °C warmer than modelled by heat diffusion alone. More recently, Seguinot et al. (2020) invoked the same process to explain measured englacial warming at a rate of 0.39 °C a^{-1} in englacial ice advancing towards the terminus of tidewater Bowdoin Glacier, Greenland. Here, it was considered that the crevasses, which possibly initiated in association with band ogives several kilometres upglacier, may have warmed the glacier's full thickness of ~250 – 300 m. Such inferences are not limited to the margins of the GrIS. For example, Gilbert et al. (2020) suggested that meltwater refreezing in crevasses may be responsible for deep warming, inferred from surface ground-penetrating radar, at Rikha Samba Glacier, Nepal, a process that may also contribute to anomalously warm englacial ice measured in boreholes across the debris-covered tongue of Khumbu Glacier, Nepal (Miles et al., 2018). Second, deep englacially terminating crevasses have also been invoked to explain englacial radar scattering. For example, Catania et al. (2008) interpreted single englacial diffractors from 1 MHz surface radar transects in Greenland as reflections from the apex of deep crevasses, in this case from depths of ~100 – 200 m (their Figure 2). Third, inferred crevasse traces have been observed in ice near the glacier bed during exploration of ice-marginal subglacial cavities and tunnels (e.g., Hubbard, Cook, & Coulson, 2009; Lovell et al., 2015), implying initial propagation to depths of greater than some tens of metres. Hambrey (1976) calculated this depth (from cumulative overburden mass loss) to be at least 80 m from observations of surface crevasse traces in the ablation area of Charles Rabots Bre, Norway. However, in these cases there is some uncertainty involved in determining confidently whether such features were originally deep surface crevasses or local basal crevasses. Finally, Fountain et al. (2005) used a borehole camera to investigate the interior of Storglaciären, Sweden, and reported the presence of water-filled englacial fractures to a depth of 131 m.

Strong inferential evidence therefore exists for the occurrence of crevasses extending >10s m below the ice surface. However, gaining direct access to such crevasses is difficult. Here, we use borehole optical televiewing to investigate the presence and properties of sub-surface crevasses at Store Glacier, a fast-moving outlet glacier of the GrIS.

2 Field site and methods

Store Glacier (Greenlandic name *Sermeq Kujalleq*) is a fast-moving outlet glacier draining the central-west sector of the GrIS into Davis Strait via Ikerasak Fjord in the Uummannaq Fiord system (Figure 1).

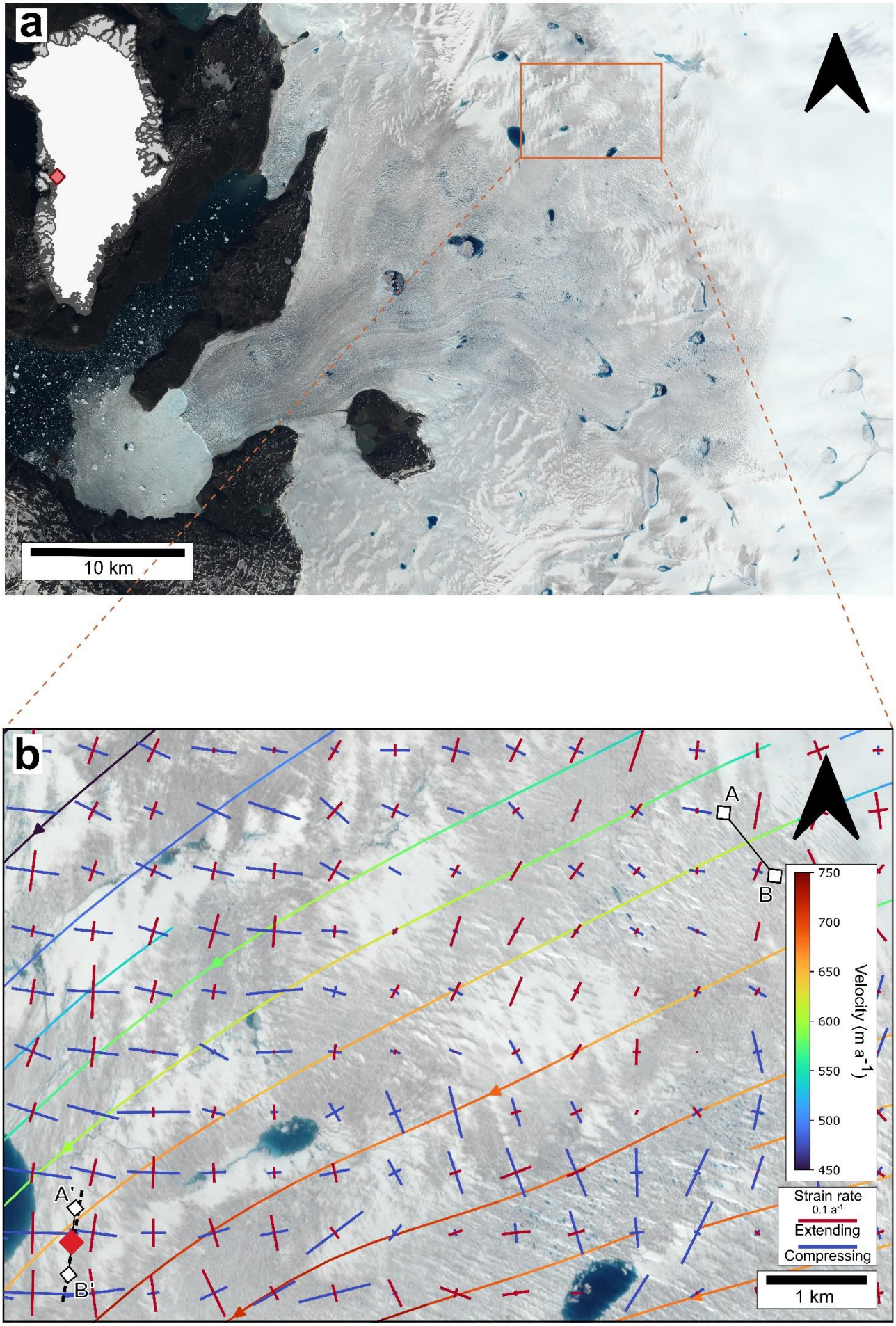
a
10 km
b
A
B
A'
B'
750
700
650
600
550
500
450
Velocity (m a-1)
Strain rate
0.1 a-1
Extending
Compressing
1 km

87

Figure 1. (a) Basemap image (Sentinel-2 taken on 07.07.2018) of Store Glacier, Greenland, and (b) expansion of (a) with layers showing: surface velocity presented as coloured flowlines; principal surface strain rates (extending in red, compressing in blue); crevasse trace azimuth from borehole OPTV (black dashed line); and crevasse rotation (A to A' and B to B') from the surface velocity field. The red diamond marks the borehole location. Surface velocity flowlines and strain rates are derived from the MEaSUREs (2017) velocity dataset (Joughin, Smith, Howat, Scambos, & Moon, 2010);

The borehole investigated herein (BH18c) was drilled in July 2018 and was located within a crevassed area ~30 km from the terminus of Store Glacier and within 1 km of a supraglacial lake that drains rapidly via hydrofracture during most summers (Chudley et al., 2019). Although the area is generally crevassed, BH18c was drilled ~5 m away from the nearest open crevasse, both for reasons of operator safety and to minimise the chances of the vertical borehole intersecting the (assumed vertical) crevasse. Locally, ice surface velocity is ~700 m a^{-1}, achieved largely through basal motion focussed at a temperate interface (Doyle et al., 2018) between ice and an underlying deformable subglacial sediment layer (Hofstede et al., 2018). Although drilling (by hot pressurized water) was halted temporarily to allow logging, the borehole was eventually drilled to the bed at a depth of ~949 m. The uppermost 325 m of this borehole was logged by optical televiewer (OPTV) on 18th July 2018, providing a geometrically accurate RGB image of the complete borehole wall at a resolution of ~1 mm both vertically and laterally. The OPTV instrument also houses a 3-axis accelerometer and a 3-axis magnetometer, enabling orientation of the image log to magnetic north. Such OPTV images have the capacity to inform on annual accumulation (Philippe et al., 2016), the presence and scale of refrozen layers within firn (Hubbard et al., 2016), marine ice accretion (Hubbard et al., 2012) and visible structural features intersecting the borehole wall (Roberson & Hubbard, 2010). For example, the last of these studies identified eight separate ice structures, including high-angle crevasse traces to a depth of some tens of metres, in the ablation area of Midre Lovénbreen, Svalbard. Since OPTV images extend around the entire (cylindrical) borehole wall, they are typically unrolled for 2D presentation, extending left to right around the compass (N-E-S-W-N or 0°-90°-180°-270°-0°). Planar layers appear as sinusoids on such 2D images, with the amplitude of the sinusoid representing the layer's dip and the phase of the sinusoid its azimuth (Hubbard, Roberson, Samyn, & Merton-Lyn, 2008). Structural analysis and plotting were carried out using software packages BiFAT (Malone, Hubbard, Merton-Lyn, Worthington, & Zwiggelaar, 2013), WellCAD, and Stereonet v.11 (Cardozo & Allmendinger, 2013). In the analysis presented herein, local declination of -30° (west) was corrected for when mapping the orientation of OPTV-imaged features. All feature azimuths are therefore presented (as three digits) clockwise from grid (NSIDC Polar Stereographic North) north.

Borehole temperatures were recorded by sensor strings installed into two boreholes, BH18b and BH18d, both located <10 m from BH18c. Englacial temperature was measured using Fenwal UNI-curve 192 thermistors (see Doyle et al., 2018) and DS18B20 digital temperature sensors (Table S1; Figure S1). Undisturbed ice temperatures were estimated following established methods (Doyle et al., 2018; Humphrey & Echelmeyer, 1990). A theoretical borehole temperature profile was also created by inverting the 2016 annually observed MEaSUREs surface ice velocity using the higher-order Community Ice Sheet Model 2.0, which conserves momentum, mass and thermal energy in three dimensions. The approach follows that used by Price et al. (2011) for Greenland and Bougamont et al. (2019) for Antarctica. The observed motion was simulated by first prescribing a no-slip basal boundary condition, and then subtracting the derived internal ice deformation from the observed surface velocities. We then iterated basal traction and sliding rates to an equilibrium in which ice temperature, effective ice viscosity, and ice velocity fields converged with the target velocities. To constrain the inversions, we used BedMachine v.3 (Morlighem et al., 2017) ice thickness and bed topography resampled to the 1 km fixed grid of our model. Surface air temperature was specified at the same 1 km resolution using output from the RACMO regional climate model (Noël et al., 2018).

3 Results

3.1 OPTV log

The complete 325 m long OPTV log of BH18c (Figure 2a) shows two general characteristics.

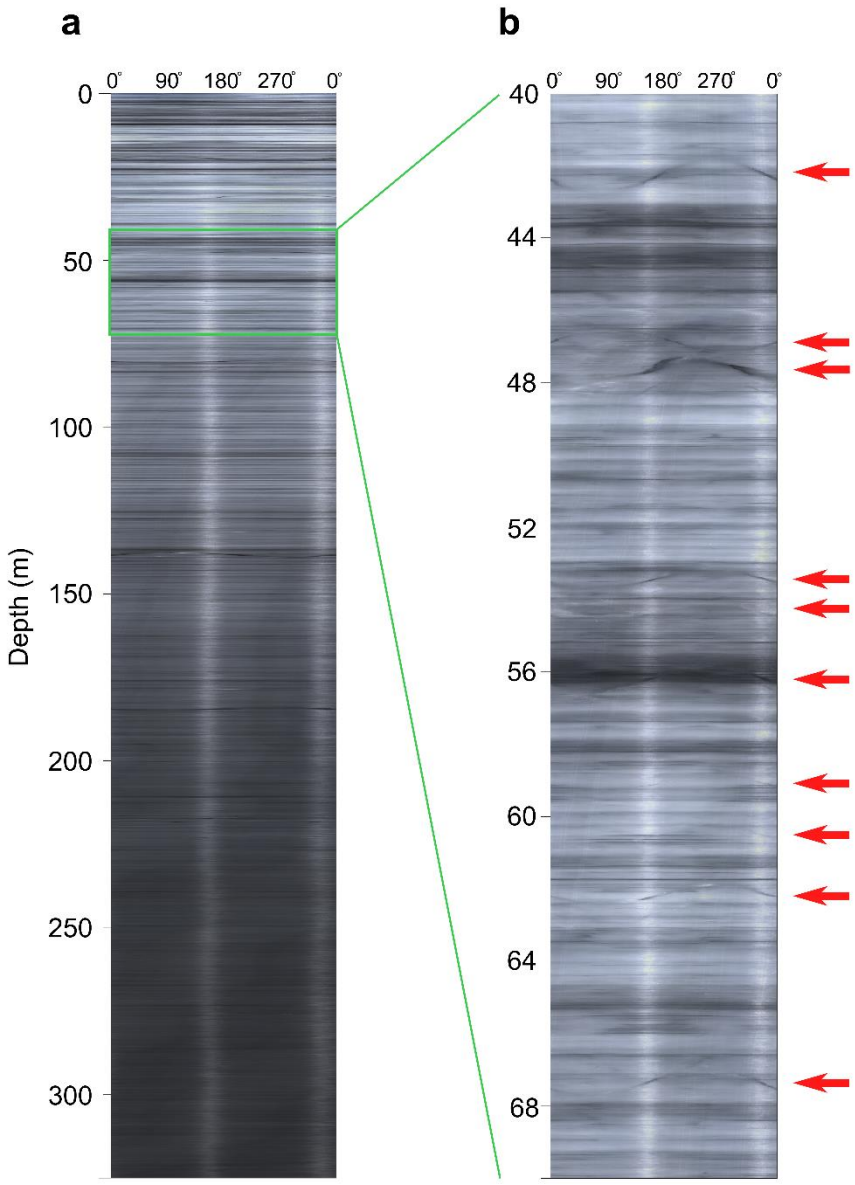

Figure 2. OPTV log of BH18c. (a) The complete 325 m-long log (note ~150 x vertical compression), and (b) expansion (~15 x vertical compression) of depth range 40 - 70 m showing 10 high angle sinusoids (planes in 3D space), each marked by a red arrow, cutting across low-angle background layers. With a borehole diameter of ~12 cm, the width of these OPTV images is the borehole circumference, ~0.38 m. The reflective (brighter) approximately vertical streaks at ~160° and ~340° are drilling artefacts, probably caused by contact between the hose and borehole wall. Images are orientated to magnetic north.

First, the log shows an overall decrease in luminosity with depth. This is common to many OPTV logs recovered from glacier boreholes (Hubbard et al., 2013), with light scattering decreasing with depth as the material forming the borehole wall progresses from highly reflective snow and firn through bubble-rich ice of intermediate reflectivity to almost transparent bubble-poor ice at depth. Since BH18c is in the ablation area of Store Glacier, it intersects no near-surface snow or firn, and the darkening in this case represents a general decrease in bubble content with depth. Second, numerous alternating decimetre-scale light and dark bands signify alternating bubble-rich 'white' ice and bubble-poor transparent ice (Figure 2b). This banding extends throughout the full depth of the OPTV log and, although appearing uniform and horizontal at the (vertically compressed) scale illustrated in Figure 2a, an expanded section (Figure 2b) reveals that the banding dips shallowly and is of variable thickness around the borehole.

Closer inspection of the OPTV log of BH18c also reveals the presence of 35 distinct high-angle layers (examples of which are indicated by red arrows in Figure 2b) that cut across the less distinct, lower-angle

banding noted above. Enlargements of the log (Figure 3) reveal that these layers form regular sinusoids, indicating uniform and planar layers in 3D space. Each layer is formed of one or more millimetre-scale laminae that are bright (reflective) and hence inferred to be bubble-rich. In 28 cases, these laminae are enveloped by centimetre- to decimetre-thick layers of ice that appear dark and are hence transparent and devoid of reflective bubbles. Of these 28 layers, 24 host a single central lamina (e.g., Figure 3a and b), one hosts two such laminae, two host three such laminae, and one (a ~0.25 m-thick layer at a depth of ~184 m) hosts nine such laminae (Figure 3c).

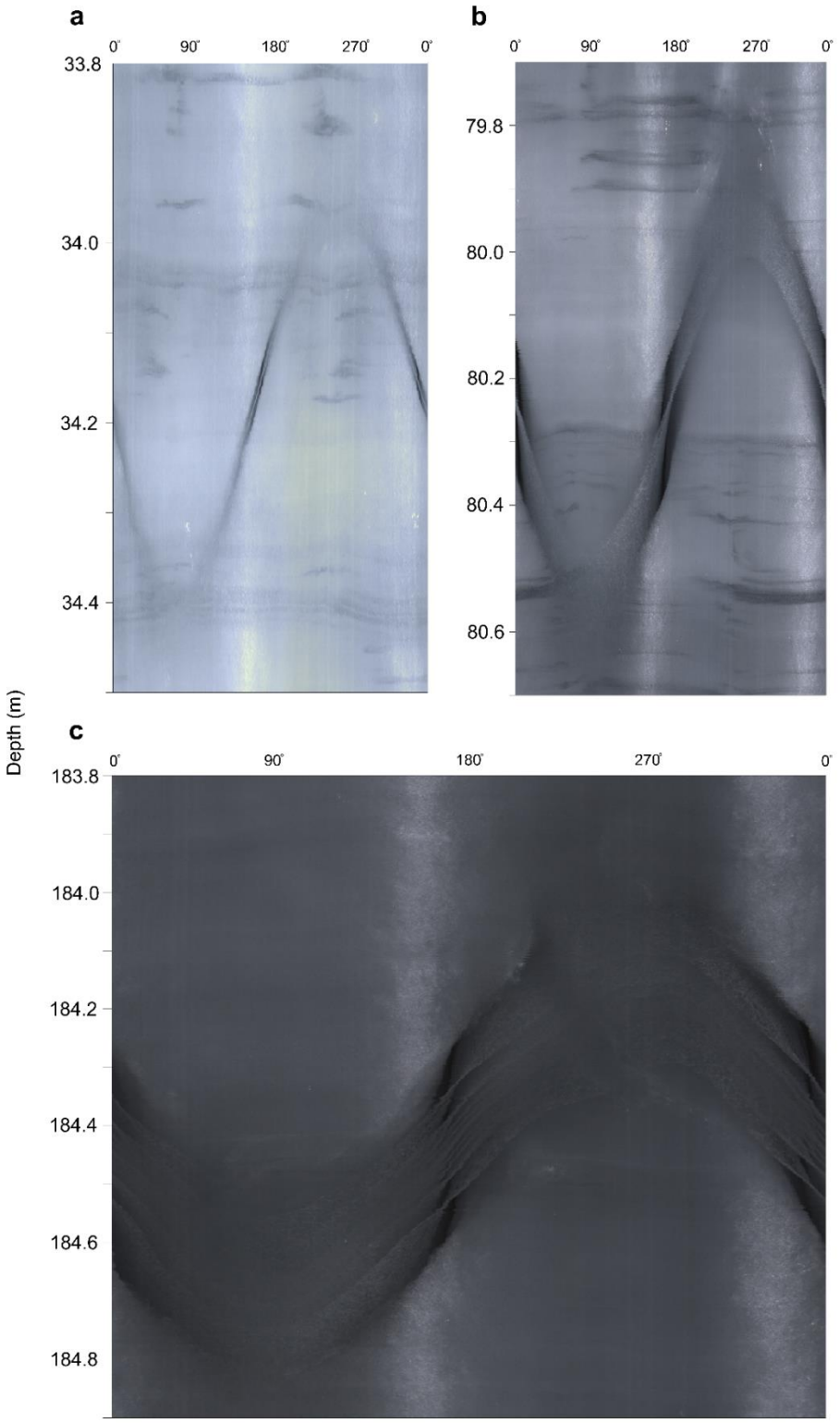

Figure 3. Selected expanded sections of the OPTV image of BH18c (shown in Figure 2), illustrating high-angle planar layers, apparent as a sinusoid in these 2D representations: (a) 33.8 – 34.5 m depth, (b) 79.7 – 80.7 m depth, and (c)

183.8 – 184.9 m depth. Note the general decrease in luminosity with depth and the central bubble-rich (bright) planar layers bisecting the high-angle layers imaged in (a) and (b) and the presence of multiple such layers in (c). Images are orientated to magnetic north.

Analysis of the distribution of the 35 high-angle layers intersected by BH18c (Figure 4a) shows a general decline in frequency with depth, with the deepest observed plane being 265 m below the glacier surface. It is quite possible that the borehole intersected similar planes below this depth but that they were indistinguishable from the background ice. This is because (visibly bright) included bubbles are progressively expelled from all ice as pressure increases with depth, homogenizing the darkening OPTV image.

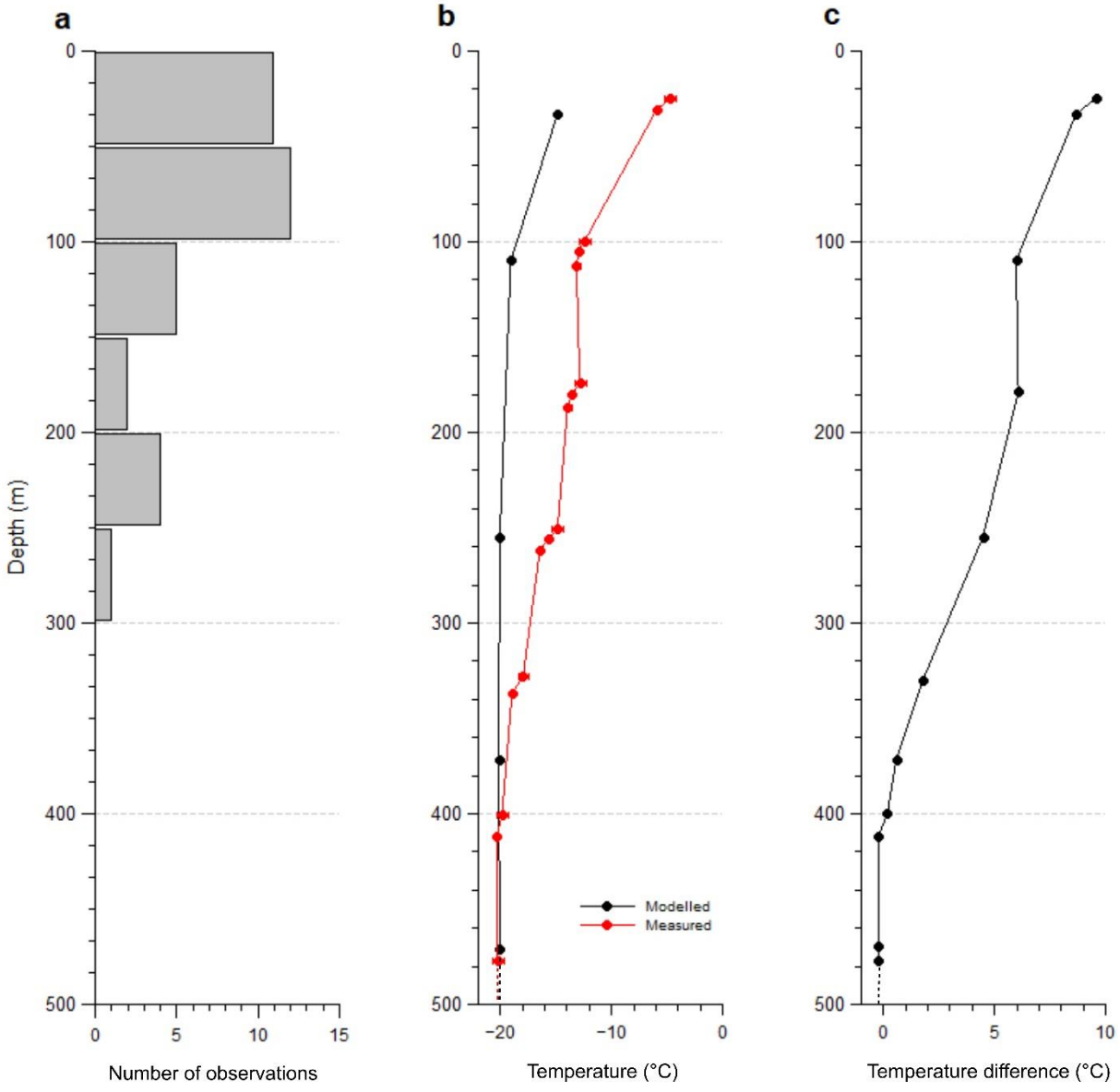

Figure 4. Key properties of the uppermost ~480 m of BH18c at Store Glacier: (a) histogram of the number of high-angle planes identified in the OPTV log (which extended to a depth of 325 m), (b) modelled (black) and measured (red) englacial temperatures for the upper half of the ice column, and (c) difference ('residual temperature') between the measured and modelled temperatures presented in (b).

Geometrical analysis of the orientation (relative to true north) of these planes reveals a strong single maximum dipping approximately WNW to ESE (mean azimuth of pole to plane = 287°) at a mean dip of 63° (Figure 5 and Table 1).

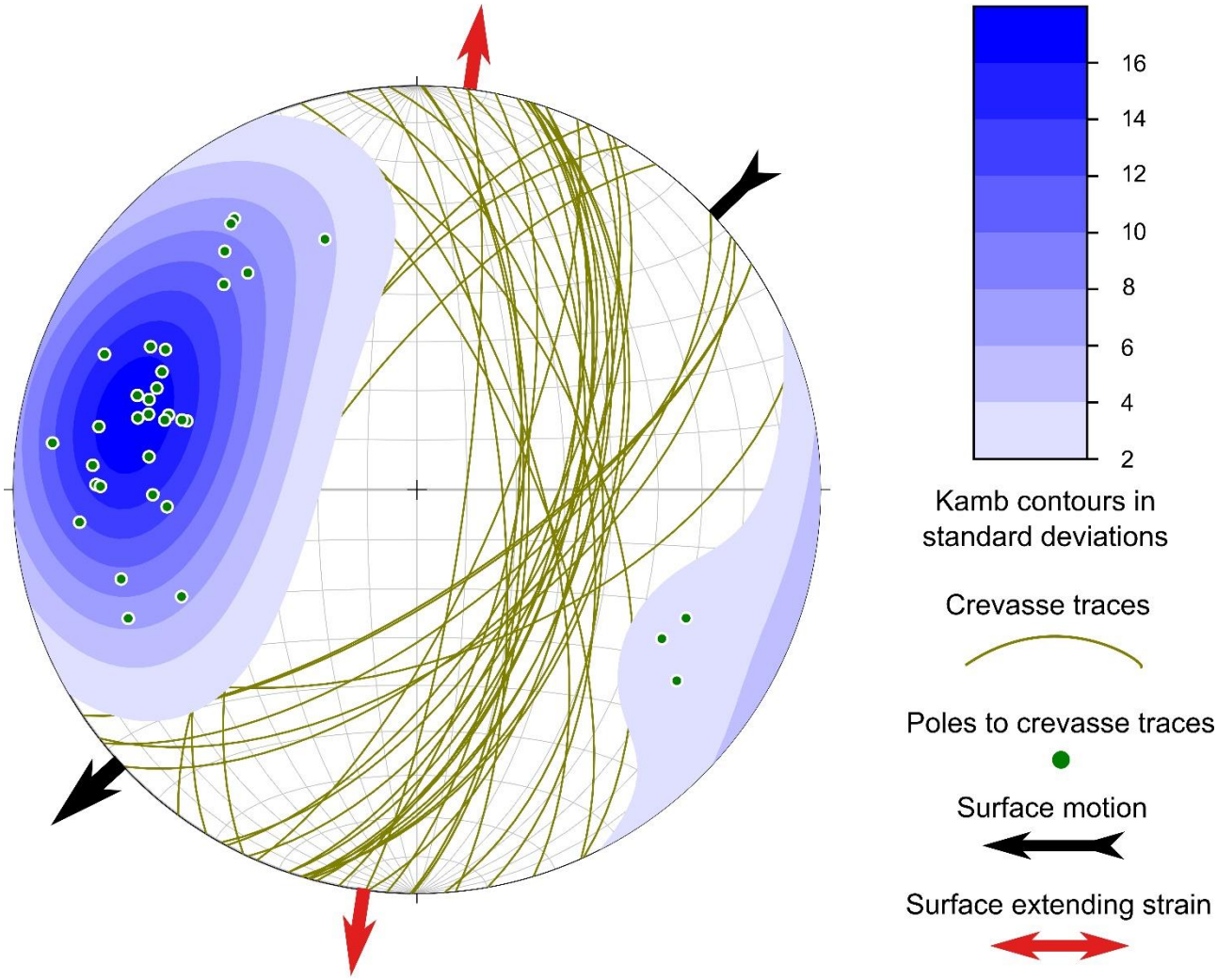

Figure 5. Lower hemisphere equal-area plot of all high-angle planes identified in the OPTV log of the uppermost 325 m of BH18c. Planes are plotted as green lines and poles to those planes as green dots, contoured by standard deviation following Kamb (1959). Eigen analysis data are given in Table 1. Note, these planes have been corrected for local declination and are orientated to grid north for consistency with Figure 1. Thick arrows give the direction of local surface motion (black) and the azimuth of local principal surface extending strain (red).

Accordingly, eigen analysis of the poles to these planes (green dots on Figure 5) indicates a strongly clustered fabric with a dominant principal eigenvalue of 0.83 at a vector of 287° (Table 1). Considering the strength of this mode, the second and third eigenvalues (of 0.1 and 0.07 respectively) have little physical meaning.

Table 1. Eigen analysis data summarizing the 3D orientation of all 35 high-angle poles to planes (orientated to grid north), plotted as dots on Figure 5, identified in the OPTV log of the uppermost 325 m of BH18c.

Axis	Eigenvalue	Eigenvector	
		Azimuth (°)	Dip (°)
1	0.83	287	63
2	0.10	190	75
3	0.07	75	31

3.2 Englacial ice temperature

The borehole sensor strings recorded 32 discrete ice temperatures between the near-surface and the ice-bed interface (Figure S1). These temperatures decrease from ~-5 °C at a depth of ~25 m (the uppermost thermistor location in the borehole) to ~-22 °C at 600 – 700 m depth, to rise again sharply to temperate at the bed at a depth of ~949 m. Over most of the borehole length, the modelled temperatures correspond closely with the measured temperatures (Figure S1). However, modelled temperatures diverge from the observed record in the depth ranges 0 – ~400 m and 770 - 850 m. The former of these is relevant to the present study, and temperature data over the depth range 0 – 500 m are plotted in Figure 4b. Here, measured temperatures are notably higher than modelled temperatures, a difference ('residual temperature') that decreases with depth from ~10 °C near the surface to zero at ~400 m (Figure 4c).

4 Interpretation and discussion

The background (host) ice is formed of alternating sub-horizontal, but irregular, bands of bright bubble-rich ice and darker bubble-poor ice at the scale of centimetres to decimetres. This is typical of the remnants of primary stratification in englacial ice, with the bands having originally been laid down as snowfall in the accumulation area of the GrIS. Such primary stratification has been identified elsewhere, both at the glacier surface (see review by Hambrey & Lawson, 2000) and within borehole OPTV logs (Roberson & Hubbard, 2010). Superimposed onto this primary structure, the high-angle planes have the physical properties of healed crevasses or crevasse traces (Hambrey & Müller, 1978). These properties include their secondary status (cutting across the primary stratification), high angle, and planar geometry. The clear nature of the transparent ice forming these layers is consistent with formation by the refreezing of a water-filled crack some cm to tens of cm across, similar in dimension to the fractures intersected by boreholes at Storglaciären, Sweden (Fountain et al., 2005). Such ice is typical of refrozen ice from which gas has been expelled during the freezing process (e.g., Pohjola, 1994), as are their bubble-rich central laminae. Here, gas is rejected at the advancing ice front, increasing its concentration in the remaining reservoir of unfrozen water, eventually reaching saturation. At that point, bubbles form and are incorporated as a lamina into the last-frozen ice layer (Hubbard, 1991). The central position of the bubble-rich last-frozen lamina we observe in most of the OPTV image of BH18c (Figures 3a and b) is consistent with water freezing inwards at a similar rate from both edges of a crevasse. Similar features, also interpreted as crevasse traces, have been identified cropping out at the glacier surface (e.g., Figure 6).

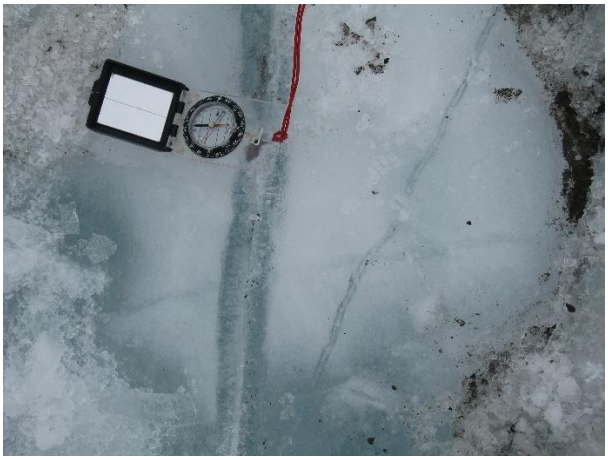

Figure 6. Photograph of a surface exposure of a set of sub-vertical crevasse traces at Trapridge Glacier, Canada (Hambrey & Clarke, 2019; their Figure 7d). Note the planar crevasse traces cut across the host ice and are generally clear with a bubble-rich central plane, like those in our OPTV images shown in Figure 3.

Where exposed at the glacier surface, such clear ice crevasse traces commonly erode preferentially, providing channels for supraglacial drainage (Hambrey & Müller, 1978) (also see Figure S2). We interpret multiple last-frozen laminae within a crevasse trace, such as that imaged at a depth of 184 m (Figure 3c), in terms of the effects of multiple separate refreezing events. Although multiple central laminae have not, to our knowledge,

been reported elsewhere, reactivation of crevasse traces as thrust faults has been proposed (e.g., Goodsell, Hambrey, Glasser, Nienow, & Mair, 2005). At Store Glacier, we envisage trace reactivation to involve opening along its bubble-rich last-frozen lamina and splitting that layer into two thinner bubble-rich laminae. The open crevasse then refills with meltwater that eventually refreezes, forming a new (third) bubble-rich last-frozen lamina. After that, any subsequent reactivation can open any of the three pre-existing last-frozen laminae and the process is repeated, each time adding a pair of new laminae and therefore generally resulting in an odd total number of such laminae. This is consistent with our observations, and in particular with the feature at 184 m depth which has nine such laminae (Figure 3c), indicating that the initial crevasse trace was reactivated four times. In contrast, we imaged one high-angle layer with an even number of central laminae (two). In this case, the crevasse could have reactivated along a new plane rather than along the pre-existing central laminae. If this were the case then, of the 28 filled crevasse traces imaged in the uppermost 325 m of BH18c, 24 showed no clear evidence of reactivation, three showed evidence of a single reactivation phase, and one showed evidence of four reactivation phases. Of these seven inferred reactivation phases, six occurred along a pre-existing bubble-rich last-frozen lamina. The seven bright laminae that were not visually bounded by transparent (refrozen) ice likely formed either as unopened fractures or as dry crevasses, the traces of which consequently did not host a refrozen ice layer.

Geometrical analysis of the crevasse traces intersected in BH18c (Figures 1b and 5) indicates a strongly clustered distribution with a dip of 63° and a strike of 017°, neither of which varies systematically with depth. Reference to Figure 1b shows that this strike differs by 87° from that of local surface crevasses, which trend ~110° (none of which was intersected by the borehole). Further, the local azimuth of principal extending strain is ~008°, so the orientation of the OPTV-imaged crevasse traces diverges by ~81° from orthogonal to this. The crevasse traces intercepted by BH18c are therefore aligned ~81° away from the azimuth at which local crevasses should form if solely by fracture Mode I 'opening' (Colgan et al., 2016). Indeed, even local open surface crevasses deviate from orthogonal to the azimuth of local principal extending strain by 12°. While the orientation of principal stress can rotate a few degrees with depth (Pfeffer, Humphrey, Amadei, Harper, & Wegmann, 2000), this offset is compatible with local surface crevasses opening under local strain conditions, with mixed mode fracture explaining the slight offset. However, the englacial traces imaged by our OPTV log are highly unlikely to have formed locally by any combination of fracture mode. This interpretation is supported by our inference of multiple trace reactivation since each such event requires three phases: (i) crevasse opening, (ii) water filling, and (iii) water freezing. It is unlikely that all three phases could occur multiple times within a single year and - although no independent evidence is currently available to evaluate this – variability in the requisite fracturing and temperatures are greatest, and therefore most likely, at the annual timescale. The traces we image - one with four reactivation phases – are therefore likely to be at least four years old, and probably older. With a local ice velocity of ~700 m a^{-1}, that places their origin at least ~3 km upglacier. Figure 1b shows the presence of two areas of opening crevasses up-flow of the borehole location, one ~4 km distant and the other ~8 km distant. Since extending strain rates are small between the first of these sites and the borehole (and crevasse reactivation is therefore unlikely along this path) this location is unlikely to serve as the origin of the traces intercepted by the borehole. In contrast, crevasses formed at the more distant site both have farther to travel (allowing more time for reactivation) and pass through the lower site of locally high extending strain rates. Indeed, plotting the trajectory of crevasse azimuth at the upper site to the borehole (illustrated by the paths of A to A' and B to B' on Figure 1b) rotates this original azimuth to within 7° of the strike of the englacial traces imaged at the borehole. We therefore consider that the most likely location for the formation of the crevasses whose traces we image by OPTV in BH18c was ~8 km upglacier (although, without further evidence, formation farther upglacier again cannot be discounted).

Figure 1b reveals that neither the crevasse field at the borehole location nor that located ~8 km upglacier is aligned orthogonal to the local azimuth of principal extending strain, suggesting mixed-mode crevasse formation at both sites (Colgan et al., 2016). The occurrence of Mode II 'sliding' and/or mode III 'tearing' is also consistent with seven of the 35 imaged traces having no discernible refrozen ice component;

in such cases the fracture either opened and closed without water ingress and freezing (considered possible but unlikely) or formed largely by Mode II and/or Mode III fracture. Certainly, Mode I 'opening' predominates, as evidenced by the (open) surface crevasses and by the presence of refrozen ice in 28 of the 35 traces we image. However, none of these crevasse traces appears to displace the pre-existing background stratification (Figure 3). While it is possible that vertical displacement of lower-than-detectable magnitude did occur, we estimate – based on the nature of the OPTV images and the irregularity of the stratification – that any such displacement would have been less than a few millimetres in all cases. We therefore consider initial crevasse formation involving a significant Mode II component as unlikely and instead favour Mode I combined with Mode III fracture at, and upglacier of, our study site.

We also note that the traces we image dip at a mean angle of 63° and show no systematic change in dip with depth. While the dip of open crevasses is difficult to measure directly for more than a few meters below the surface, shallowly dipping crevasse traces have been reported from valley glaciers. For example, Roberson and Hubbard (2010) identified transverse fractures (their 'S2') in OPTV borehole logs from midre Lovénbreen, Svalbard, which dipped as shallowly as 60°. Similarly, Hambrey and Müller (1978) mapped several sets of crevasse traces exposed at the surface of White Glacier, Canada. This mapping showed that crevasse traces were typically near vertical ~3 km upglacier from the terminus, but that they dipped progressively as they advected downglacier until they became almost horizontal at the terminus. It is not therefore uncommon for crevasse traces to dip as they advect through an ice mass. That the primary stratification has remained close to horizontal in our OPTV images at Store Glacier (Figures 2 and 3) suggests that the crevasse traces have dipped without rotating the pre-existing stratification; thus the crevasses either formed initially at a mean dip of 63°, or formed vertically and subsequently became less steep under simple shear. If the latter, then the mean trace dip of 63° at the borehole site also supports our interpretation that the antecedent crevasses formed several kilometres upglacier. Initially vertical crevasse formation, followed by strain-induced shallowing during passage along the glacier, is also consistent with BH18c not intersecting any local crevasses, despite them being only some metres distant at the glacier surface.

It takes ~40 years for ice to move from the borehole location to the front of Store Glacier, during which time ~100 m of surface ice would be lost to ablation (assuming a surface ablation rate of 2.5 m a^{-1}). Thus, crevasse traces deeper than this at the borehole site, as well as those formed deep enough farther down-glacier, would survive to the glacier's terminus, some to depths of 100s of metres. Given several of the crevasse traces we report herein show evidence of reactivation – implying they are weaker than adjacent host ice – and the continued formation of similar crevasses downglacier, nearer to the terminus, it is possible that crevasse traces reaching the terminus present sub-vertical planes of weakness there, offering locations of preferential fracture. If this is the case, then models of fracture mechanics may need to account for the presence of such deep and geometrically recurring planes of weakness.

The frequency of intersected crevasse traces shows a general decrease with depth (Figure 4a), consistent with their antecedent crevasses forming at the surface and terminating at different depths. Assuming this depth distribution represents that of the original crevasses, then only seven (or 20%) of the 35 intersected by the borehole were shallower than 40 m depth and 12 (34%) were deeper than 100 m. Although specific to our study site, the relationship between the crevasses present (%) per 30 m depth range ($C(30)_{\%}$) and depth (D, m), as illustrated in Figure 4a, can be approximated (R = 0.69) as a logarithmic function:

$$C(30)_{\%} = 40 - 6.2\ln(D) \qquad \text{Eq. 1}$$

This fit both suggests the presence of crevasses below the lowermost crevasse trace imaged by our OPTV log (at a depth of 265 m) and is consistent with the difference between measured and modelled englacial temperatures at our field site (Figure 4c), suggesting that crevasses warmed englacial ice to a depth of at least ~400 m. Fitting a logarithmic curve to this residual temperature (T_e, °C) against depth, as illustrated in Figure 4c, yields a close match (R = 0.95) described by:

$$T_e = 21.0 - 3.3\ln(D) \qquad \text{Eq. 2}$$

The similarity of the relationships between crevasse frequency and depth (Figure 4a; Eq. 1) and residual temperature and depth (Figure 4c; Eq. 2) lends support to our interpretation that crevasses propagate to at least 400 m below the surface of Store Glacier, warming ice to that depth by the presence and refreezing of crevasse-filling meltwater.

5 Summary and conclusions

Our OPTV log of a borehole drilled in a crevassed area of fast-moving Store Glacier, Greenland, has successfully imaged deep crevasses in the GrIS for the first time. Combining analysis of this log with thermo-mechanical modelling has revealed the following.

- Thirty-five traces of surface crevasses were imaged directly to a maximum depth of 265 m. It is possible that the borehole intersected crevasses below this, but that they could not be distinguished from the host ice. Although trace separation increased with depth, approximately one third of all traces were intersected below a depth of 100 m.
- The borehole intersected traces of crevasses that were highly unlikely to have formed locally. Comparison of trace orientation with the surface strain rate field of Store Glacier indicates their antecedent crevasses most likely formed ~8 km upglacier.
- Despite drilling in an active crevasse field, and between two open crevasses spaced ~10 m apart, the borehole intersected no local crevasses. This indicates that the active local crevasses were shallow and/or did not deviate sufficiently from vertical to intersect the uppermost 325 m of the borehole.
- Crevasse fields analysed are not aligned perpendicular to the orientation of principal extending strain rate, indicating mixed-mode formation, likely Modes I and III since the traces did not appear to displace primary stratification vertically.
- Of the 35 traces imaged, 28 showed evidence of having been filled with meltwater that subsequently refroze. This meltwater and its refreezing released heat, assumed to be responsible for warming the ice to a depth of ~400 m, suggesting crevasses extended to this depth - although not imaged below 265 m by our OPTV log.
- Refreezing of crevasse-fill water creates a distinctive ice layer formed of a planar bubble-free ice layer some centimetres to decimetres thick that envelopes a planar mm-thick central layer of bubble-rich last-frozen ice.
- We hypothesize that, once formed, crevasse traces represent a plane of weakness that may be reactivated during advection through the glacier. Visual analysis of the traces imaged by borehole OPTV suggests that reopening occurs preferentially along the bubble-rich last-frozen layer(s), which then refill and refreeze, creating additional new last-frozen layers. The time required for crevasse opening, filling and refreezing is not known but is likely to be some years, consistent with the ~8 km distance separating the borehole from the proposed location of initial crevasse formation.
- The crevasse traces imaged by our OPTV log, supplemented by new ones formed downglacier, extend deep enough to survive ablation and reach the glacier terminus. Here, it is possible that these relatively weak traces precondition the precise location of ice fracture, a process that may need to be addressed by fracture models.

Acknowledgments

This research was funded by the European Research Council as part of the RESPONDER project under the European Union's Horizon 2020 research and innovation program (Grant 683043). Hot water drilling and borehole logging equipment were also supported by an Aberystwyth University Capital Equipment Grant and NERC grants NE/J013544 and NE/K610026. TRC and RL were supported by a UK NERC Doctoral Training Partnership Studentship (Grant NE/L002507/1). We are grateful to Ann Andreasen and the Uummannaq Polar Institute for their kind hospitality, to Nicole Bienert and Sean Peters for assistance in the field, and to Katie Miles, Emma Docherty and Tom Chase for assistance in constructing sensor strings.

Data availability

The OPTV image and measured and modelled englacial temperature data presented herein are available from https://doi.org/10.6084/m9.figshare.13400072.v1

References

Boon, S., & Sharp, M. (2003). The role of hydrologically-driven ice fracture in drainage system evolution on an Arctic glacier. *Geophysical Research Letters, 30*(18). doi:10.1029/2003gl018034

Bougamont, M., Christoffersen, P., Nias, I., Vaughan, D. G., Smith, A. M., & Brisbourne, A. (2019). Contrasting Hydrological Controls on Bed Properties During the Acceleration of Pine Island Glacier, West Antarctica. *Journal of Geophysical Research: Earth Surface, 124*(1), 80-96. doi:10.1029/2018jf004707

Cardozo, N., & Allmendinger, R. W. (2013). Spherical projections with OSXStereonet. *Computers & Geosciences, 51*, 193-205. doi:https://doi.org/10.1016/j.cageo.2012.07.021

Catania, G. A., Neumann, T. A., & Price, S. F. (2008). Characterizing englacial drainage in the ablation zone of the Greenland ice sheet. *Journal of Glaciology, 54*(187), 567-578. doi:10.3189/002214308786570854

Chudley, T. R., Christoffersen, P., Doyle, S. H., Bougamont, M., Schoonman, C. M., Hubbard, B., & James, M. R. (2019). Supraglacial lake drainage at a fast-flowing Greenlandic outlet glacier. *Proceedings of the National Academy of Sciences*, 201913685. doi:10.1073/pnas.1913685116

Colgan, W., Rajaram, H., Abdalati, W., McCutchan, C., Mottram, R., Moussavi, M. S., & Grigsby, S. (2016). Glacier crevasses: Observations, models, and mass balance implications. *Reviews of Geophysics, 54*(1), 119-161. doi:doi:10.1002/2015RG000504

Colgan, W., Steffen, K., McLamb, W. S., Abdalati, W., Rajaram, H., Motyka, R., . . . Anderson, R. (2011). An increase in crevasse extent, West Greenland: Hydrologic implications. *Geophysical Research Letters, 38*(18). doi:10.1029/2011gl048491

Das, S. B., Joughin, I., Behn, M. D., Howat, I. M., King, M. A., Lizarralde, D., & Bhatia, M. P. (2008). Fracture Propagation to the Base of the Greenland Ice Sheet During Supraglacial Lake Drainage. *Science, 320*(5877), 778-781. doi:10.1126/science.1153360

Doyle, S. H., Hubbard, A. L., Dow, C. F., Jones, G. A., Fitzpatrick, A., Gusmeroli, A., . . . Box, J. E. (2013). Ice tectonic deformation during the rapid in situ drainage of a supraglacial lake on the Greenland Ice Sheet. *The Cryosphere, 7*(1), 129-140. doi:10.5194/tc-7-129-2013

Doyle, S. H., Hubbard, B., Christoffersen, P., Young, T. J., Hofstede, C., Bougamont, M., . . . Hubbard, A. (2018). Physical Conditions of Fast Glacier Flow: 1. Measurements From Boreholes Drilled to the Bed of Store Glacier, West Greenland. *Journal of Geophysical Research: Earth Surface, 123*. doi:10.1002/2017JF004529

Fountain, A. G., Jacobel, R. W., Schlichting, R., & Jansson, P. (2005). Fractures as the main pathways of water flow in temperate glaciers. *Nature, 433*(7026), 618-621. doi:10.1038/nature03296

Gilbert, A., Sinisalo, A., Gurung, T. R., Fujita, K., Maharjan, S. B., Sherpa, T. C., & Fukuda, T. (2020). The influence of water percolation through crevasses on the thermal regime of a Himalayan mountain glacier. *The Cryosphere, 14*(4), 1273-1288. doi:10.5194/tc-14-1273-2020

Goodsell, B., Hambrey, M. J., Glasser, N. F., Nienow, P., & Mair, D. (2005). The structural glaciology of a temperate valley glacier: Haut Glacier d-'Arolla, Valais, Switzerland. *Arctic Antarctic and Alpine Research, 37*(2), 218-232. Retrieved from <Go to ISI>://WOS:000229484200010

Hambrey, M. J. (1976). Structure of the glacier Charles Rabots Bre, Norway. *GSA Bulletin, 87*(11), 1629-1637. doi:10.1130/0016-7606(1976)87<1629:Sotgcr>2.0.Co;2

Hambrey, M. J., & Clarke, G. K. C. (2019). Structural Evolution During Cyclic Glacier Surges: 1. Structural Glaciology of Trapridge Glacier, Yukon, Canada. *Journal of Geophysical Research: Earth Surface, 124*(2), 464-494. doi:10.1029/2018jf004869

Hambrey, M. J., & Lawson, W. (2000). Structural styles and deformation fields in glaciers: a review. *Geological Society, London, Special Publications, 176*(1), 59-83. doi:10.1144/gsl.Sp.2000.176.01.06

Hambrey, M. J., & Müller, F. (1978). Structures and Ice Deformation in the White Glacier, Axel Heiberg Island, Northwest Territories, Canada. *Journal of Glaciology, 20*(82), 41-66. doi:10.3189/S0022143000021213

Hofstede, C., Christoffersen, P., Hubbard, B., Doyle, S. H., Young, T. J., Diez, A., . . . Hubbard, A. (2018). Physical Conditions of Fast Glacier Flow: 2. Variable Extent of Anisotropic Ice and Soft Basal Sediment From Seismic Reflection Data Acquired on Store Glacier, West Greenland. *Journal of Geophysical Research: Earth Surface, 123*. doi:10.1002/2017jf004297

Hubbard, B. (1991). Freezing-rate effects on the physical characteristics of basal ice formed by net adfreezing. *Journal of Glaciology, 37*(127), 339-347. doi:10.3189/S0022143000005773

Hubbard, B., Cook, S., & Coulson, H. (2009). Basal ice facies: a review and unifying approach. *Quaternary Science Reviews, 28*, 1956-1969. doi:10.1016/j.quascirev.2009.03.005

Hubbard, B., Luckman, A., Ashmore, D. W., Bevan, S., Kulessa, B., Kuipers Munneke, P., . . . Rutt, I. (2016). Massive subsurface ice formed by refreezing of ice-shelf melt ponds. *Nature Communications, 7*, 11897. doi:10.1038/ncomms11897

Hubbard, B., Roberson, S., Samyn, D., & Merton-Lyn, D. (2008). Digital optical televiewing of ice boreholes. *Journal of Glaciology, 54*(188), 823-830. doi:10.3189/002214308787779988

Hubbard, B., Tison, J.-L., Pattyn, F., Dierckx, M., Boereboom, T., & Samyn, D. (2012). Optical-televiewer-based identification and characterization of material facies associated with an Antarctic ice-shelf rift. *Annals of Glaciology, 53*(60), 137-146.

Hubbard, B., Tison, J.-L., Philippe, M., Heene, B., Pattyn, F., Malone, T., & Freitag, J. (2013). Ice-shelf density reconstructed from optical-televiewer borehole logging. *Geophysical Research Letters*, 2013GL058023. doi:10.1002/2013gl058023

Humphrey, N., & Echelmeyer, K. (1990). Hot-water drilling and borehole closure in cold ice. *Journal of Glaciology, 36*(124), 287-298. Retrieved from <Go to ISI>://A1990EQ92000005

Joughin, I., Smith, B. E., Howat, I. M., Scambos, T., & Moon, T. (2010). Greenland flow variability from ice-sheet-wide velocity mapping. *Journal of Glaciology, 56*(197), 415-430. doi:10.3189/002214310792447734

Kamb, W. B. (1959). Ice petrofabric observations from Blue Glacier, Washington, in relation to theory and experiment. *Journal of Geophysical Research (1896-1977), 64*(11), 1891-1909. doi:10.1029/JZ064i011p01891

Lovell, H., Fleming, E. J., Benn, D. I., Hubbard, B., Lukas, S., & Naegeli, K. (2015). Former dynamic behaviour of a cold-based valley glacier on Svalbard revealed by basal ice and structural glaciology investigations. *Journal of Glaciology, 61*(226), 309-328.

Lüthi, M. P., Ryser, C., Andrews, L. C., Catania, G. A., Funk, M., Hawley, R. L., . . . Neumann, T. A. (2015). Heat sources within the Greenland Ice Sheet: dissipation, temperate paleo-firn and cryo-hydrologic warming. *The Cryosphere, 9*(1), 245-253. doi:10.5194/tc-9-245-2015

Malone, T., Hubbard, B., Merton-Lyn, D., Worthington, P., & Zwiggelaar, R. (2013). Borehole and Ice Feature Annotation Tool (BIFAT): A program for the automatic and manual annotation of glacier borehole images. *Computers & Geosciences, 51*(0), 381-389. doi:http://dx.doi.org/10.1016/j.cageo.2012.09.002

Miles, K. E., Hubbard, B., Quincey, D. J., Miles, E. S., Sherpa, T. C., Rowan, A. V., & Doyle, S. H. (2018). Polythermal structure of a Himalayan debris-covered glacier revealed by borehole thermometry. *Scientific Reports, 8*(1). doi:10.1038/s41598-018-34327-5

Morlighem, M., Williams, C. N., Rignot, E., An, L., Arndt, J. E., Bamber, J. L., . . . Zinglersen, K. B. (2017). BedMachine v3: Complete Bed Topography and Ocean Bathymetry Mapping of Greenland From Multibeam Echo Sounding Combined With Mass Conservation. *Geophysical Research Letters, 44*(21), 11,051-011,061. doi:10.1002/2017gl074954

Mottram, R. H., & Benn, D. I. (2009). Testing crevasse-depth models: a field study at Breiðamerkurjökull, Iceland. *Journal of Glaciology, 55*(192), 746-752. doi:10.3189/002214309789470905

Noël, B., van de Berg, W. J., van Wessem, J. M., van Meijgaard, E., van As, D., Lenaerts, J. T. M., . . . van den Broeke, M. R. (2018). Modelling the climate and surface mass balance of polar ice sheets using RACMO2 – Part 1: Greenland (1958–2016). *The Cryosphere, 12*(3), 811-831. doi:10.5194/tc-12-811-2018

Nye, J. F. (1955). Comments on Dr. Loewe's Letter and Notes on Crevasses. *Journal of Glaciology, 2*(17), 512-514. doi:10.3189/S0022143000032652

Pfeffer, W. T., Humphrey, N. F., Amadei, B., Harper, J., & Wegmann, J. (2000). In situ stress tensor measured in an Alaskan glacier. *Annals of Glaciology, 31*, 229-235. doi:10.3189/172756400781820354

Philippe, M., Tison, J.-L., Fjøsne, K., Hubbard, B., Kjær, H. A., Lenaerts, J. T. M., . . . Pattyn, F. (2016). Ice core evidence for a 20th century increase in surface mass balance in coastal Dronning Maud Land, East Antarctica. *The Cryosphere, 10*(5), 2501-2516. doi:10.5194/tc-10-2501-2016

Phillips, T., Rajaram, H., & Steffen, K. (2010). Cryo-hydrologic warming: A potential mechanism for rapid thermal response of ice sheets. *Geophysical Research Letters, 37*(20). doi:10.1029/2010gl044397

478 Pohjola, V. A. (1994). Tv-video observations of englacial voids in Storglaciären, Sweden. *Journal of Glaciology, 40*(135), 231-240.
479
480 Poinar, K., Joughin, I., Lilien, D., Brucker, L., Kehrl, L., & Nowicki, S. (2017). Drainage of Southeast Greenland
481 Firn Aquifer Water through Crevasses to the Bed. *Frontiers in Earth Science, 5*(5).
482 doi:10.3389/feart.2017.00005
483 Price, S. F., Payne, A. J., Howat, I. M., & Smith, B. E. (2011). Committed sea-level rise for the next century
484 from Greenland ice sheet dynamics during the past decade. *Proceedings of the National Academy of*
485 *Sciences*. doi:10.1073/pnas.1017313108
486 Roberson, S., & Hubbard, B. (2010). Application of borehole optical televiewing to investigating the 3-D
487 structure of glaciers: implications for the formation of longitudinal debris ridges, midre Lovenbreen,
488 Svalbard. *Journal of Glaciology, 56*(195), 143-156. doi:10.3189/002214310791190802
489 Seguinot, J., Funk, M., Bauder, A., Wyder, T., Senn, C., & Sugiyama, S. (2020). Englacial Warming Indicates
490 Deep Crevassing in Bowdoin Glacier, Greenland. *Frontiers in Earth Science, 8*(65).
491 doi:10.3389/feart.2020.00065
492 van der Veen, C. J. (1998). Fracture mechanics approach to penetration of surface crevasses on glaciers. *Cold*
493 *Regions Science and Technology, 27*(1), 31-47. doi:https://doi.org/10.1016/S0165-232X(97)00022-0
494 Weertman, J. (1973). Can a water-filled crevasse reach the bottom surface of a glacier? *IAHS Publ., 95*, 139-
495 145.

496